Biomaterials 35 (2014) 3005–3014

Contents lists available at ScienceDirect

Biomaterials

journal homepage: www.elsevier.com/locate/biomaterials

Anti-tumor efficacy of c(RGDfK)-decorated polypeptide-based micelles co-loaded with docetaxel and cisplatin

Wantong Song [a], Zhaohui Tang [a,*], Dawei Zhang [a], Ying Zhang [a], Haiyang Yu [a], Mingqiang Li [a,b], Shixian Lv [a,b], Hai Sun [a], Mingxiao Deng [c], Xuesi Chen [a]

[a] Key Laboratory of Polymer Ecomaterials, Changchun Institute of Applied Chemistry, Chinese Academy of Sciences, Changchun 130022, PR China
[b] University of Chinese Academy of Sciences, Beijing 100039, PR China
[c] Department of Chemistry, Northeast Normal University, Changchun 130021, PR China

ARTICLE INFO

Article history:
Received 6 November 2013
Accepted 10 December 2013
Available online 2 January 2014

Keywords:
Anti-tumor
C(RGDfK)
Target
Combination
Drug delivery

ABSTRACT

There are two important obstacles for the currently applied anti-cancer drug delivery systems. One is the conflict between long-circulation and cellular uptake while the other one is the achievement of ideal anti-cancer efficacy. To solve these problems, we designed a polypeptide-based micelle system that combined the advantages of receptor mediated endocytosis and multi-drug delivery. Firstly, an amphiphilic PLG-*g*-Ve/PEG graft copolymer was prepared by grafting α-tocopherol (Ve) and polyethylene glycol (PEG) to poly(L-glutamic acid) (PLG). Then docetaxel (DTX) and cisplatin (CDDP) were co-loaded into the PLG-*g*-Ve/PEG micelles via hydrophobic and chelation effect. After that, the surface of the dual-drug-loaded micelles was decorated with an $\alpha_v\beta_3$ integrin targeting peptide c(RGDfK). The targeted dual-drug-loaded micelles showed synergistic cytotoxicity and enhanced internalization rate in mouse melanoma (B16F1) cells. *In vivo* tests demonstrated that remarkable long circulation, anti-tumor and anti-metastasis efficacy could be achieved using this drug delivery system. This work revealed a strategy for the design and preparation of anti-cancer drug delivery systems with reduced side effect, enhanced anti-tumor and anti-metastasis efficacy.

1. Introduction

Advancement in nanotechnology provided enormous opportunities for anti-cancer drug delivery [1,2]. By the entrapment of anti-cancer drugs in nanocarriers, the systemic toxicity of free drugs can be reduced, and the resultant nano-drugs can passively accumulate in tumor tissue via the enhanced permeability and retention (EPR) effect [3–5]. Based on this, nano-sized anti-cancer drugs like DOXIL (doxorubicin HCl liposome injection) [6], Abraxane (paclitaxel protein-bound particles for injectable suspension) [7], and Genexol-PM (paclitaxel-loaded polymeric micelle) [8] et al. have been clinically approved for cancer treatment, and many others have entered into clinical trials [9,10].

However the currently applied anti-cancer nanomedicines are far from perfect. Although the toxicity is greatly reduced and the drug distribution in tumor is increased, the therapeutic efficacy has not been significantly improved as compared to free drugs [11,12]. There are two most essential reasons for this phenomenon. One is that the widely used pegylation strategy significantly hinders the nanomedicines from entering tumor cells, though pegylation can improve the pharmacokinetics of nanoparticles and escape the surveillance of immune cells and the reticuloendothelial system (RES) [13]. For example, the pegylated liposome-encapsulated form of doxorubicin DOXIL significantly prolonged the blood circulation time of doxorubicin (the AUC for DOXIL is >60 times that of free doxorubicin in rats) and resulted in increased intratumoral doxorubicin accumulation via the EPR effect in 48 h [14]. However, this did not come with significantly improved anti-tumor efficacy. It's found that the liposomes accumulated in tumor tissue just stayed outside tumor cells [15,16]. Another problem is the treatment with a single drug often encounters multi-drug resistance, and this greatly discounts the tumor inhibition effect [17,18].

Receptor-mediated endocytosis is an effective way for enhancing drug uptake rate. Tumor cells often overexpress some specific receptors, therefore, receptor-mediated uptake can be achieved by decorating corresponding ligands on the surface of nanocarriers, and this would relax the conflict between long circulation and drug uptake [19]. For example, a prostate-specific membrane antigen (PSMA)-targeted docetaxel nanoparticle formulation showed long blood circulation time of about 20 h,

* Corresponding author.
E-mail address: ztang@ciac.ac.cn (Z. Tang).

0142-9612/$ – see front matter © 2013 Elsevier Ltd. All rights reserved.
http://dx.doi.org/10.1016/j.biomaterials.2013.12.018

enhanced tumor accumulation and markedly better anti-tumor efficacy even at doses below the commonly applied docetaxel dose in clinic. This drug formulation has entered clinical trials [20]. Combination of two or more drugs with different action mechanisms is a promising strategy for overcoming multi-drug resistance and enhancing anti-cancer efficacy [21–23]. In particular, the nanocarrier-based drug combination, not only inherited the advantage of reducing toxicity, but also ensured the same *in vivo* route and better synergistic efficacy [23–26].

To the best of our knowledge, there are very few works applying the above mentioned two strategies of the "receptor-mediated cellular uptake" and "combination of multi-drugs" in one nanosystem. A receptor-targeted multi-drug-loaded nanomedicine would solve the two obstacles of the current nanomedicines and must result in enhanced anti-tumor efficacy. By now, only one try by Kolshetti et al. has reported a self-assembled polymeric nanoparticle platform to target and codelivery of drugs to cancer cells. In the system, polylactide conjugated with platinum(IV) prodrug was co-assembled with PLGA-PEG-COOH in the presence of docetaxel. A10 aptamer that could bind to the PSMA was derivatized on the surface of the nanoparticles. *In vitro* toxicity demonstrated the superiority of the targeted dual-drug combination nanoparticles over single-drug or non-targeted nanoparticles [27]. However, the stability of the co-assembled micelles was dubious, and there was no *in vivo* result to confirm the performance of this kind of drug delivery systems.

In this study, we presented a drug delivery system for targeted drug combination (Scheme 1). To achieve this, an amphiphilic graft copolymer PLG-*g*-Ve/PEG was prepared, microtubule-stabilizing agent docetaxel (DTX) was loaded in the inner core of the formed micelles, DNA-cross-linking agent cisplatin (CDDP) was loaded at the middle shell, which also provided a cross-linking effect for enhancing the stability of the micelles. An $\alpha_v\beta_3$ integrin targeting peptide c(RGDfK) was decorated on the surface of the dual-drug-loaded micelles. The *in vitro* synergistic cytotoxicity, endocytosis, *in vivo* fate, anti-tumor and anti-metastasis efficacy were evaluated on B16 melanoma.

2. Materials and methods

2.1. Materials

γ-Benzyl-L-glutamate-N-carboxyanhydride (BLG-NCA) was prepared on the method similar to our previous work [28]. Methoxypolyethylene glycol (mPEG, $M_n = 5000$) was bought from Sigma–Aldrich. Maleimide-polyethylene glycol (MAL-PEG-OH, $M_w = 3500$) was bought from Beijing Jenkem Technology Co., Ltd. α-Tocopherol (Vitamin E, Ve) was purchased from Alfa Aesar. Fluorescein isothiocyanate (FITC) was bought from Aladdin Reagent Co., Ltd. Docetaxel (DTX) was purchased from Beijing Huafeng United Technology Corporation. Cisplatin was purchased from Shandong Boyuan Chemical Company. c(RGDfK) was custom-made by Apeptide Co. Ltd. (Shanghai, China). N,N-dimethylformamide (DMF) was stored over calcium hydride (CaH_2) and purified by vacuum distillation with CaH_2. All the other reagents and solvents were purchased from Sinopharm Chemical Reagent Co., Ltd. and used as received.

2.2. Preparation of the graft-copolymer

The preparation and fluorescent labeling of the graft-copolymer were carried out following the method shown in Scheme 2.

2.2.1. Synthesis of poly(L-glutamic acid) (PLG)

Poly(L-glutamic acid) was prepared by ring opening polymerization of BLG-NCA followed by deprotection of the benzyl group. Briefly, BLG-NCA (26.33 g, 100 mmol) was dissolved in 270.0 mL DMF, then 1.0 mL of *n*-hexylamine (*n*-HA, 1.0 mM in DMF)

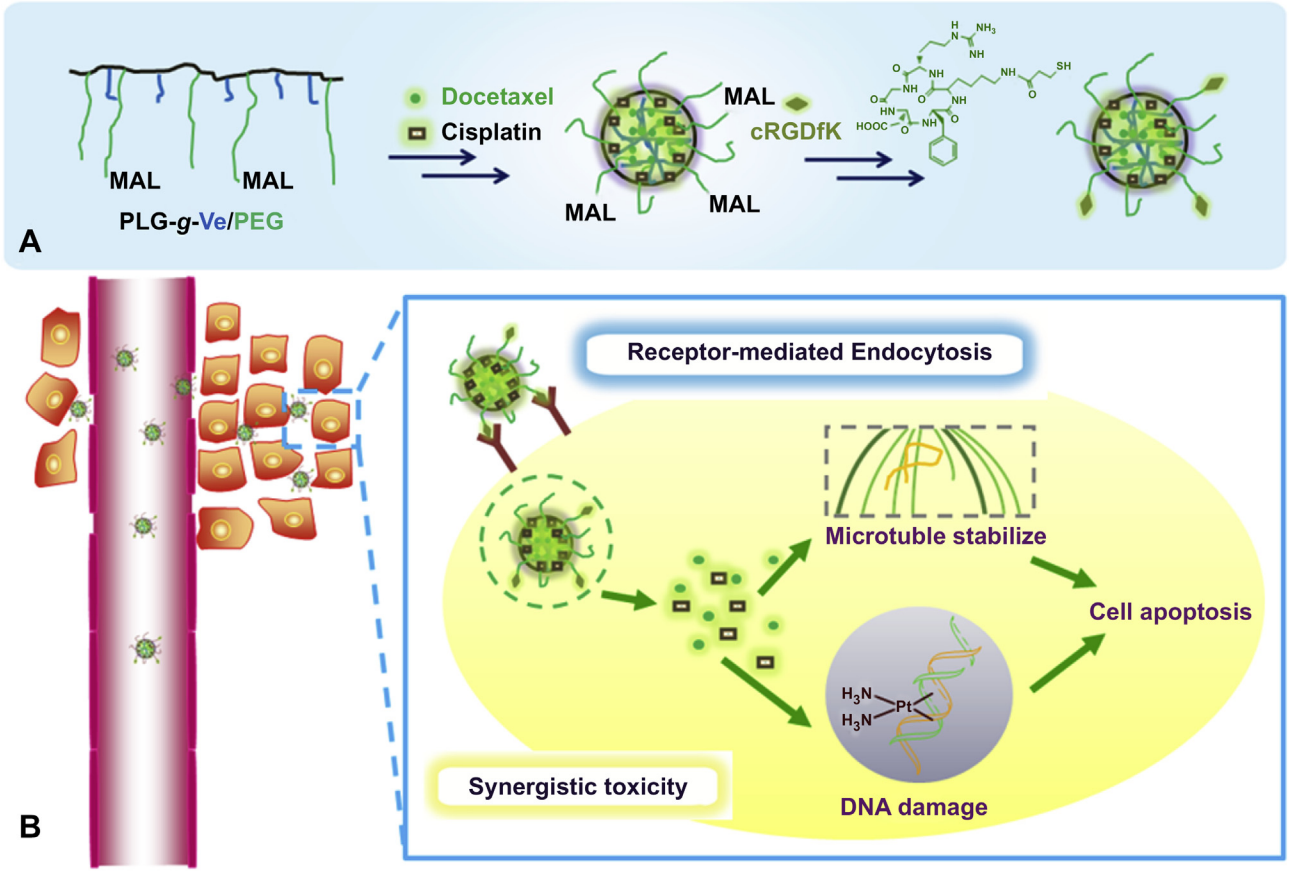

Scheme 1. (A) Schematic illustration of preparation of the c(RGDfK)-decorated dual-drug-loaded micelles. (B) The micelles enter tumor cells by receptor-mediated endocytosis, and the loaded two drugs act synergistically intracellularly.

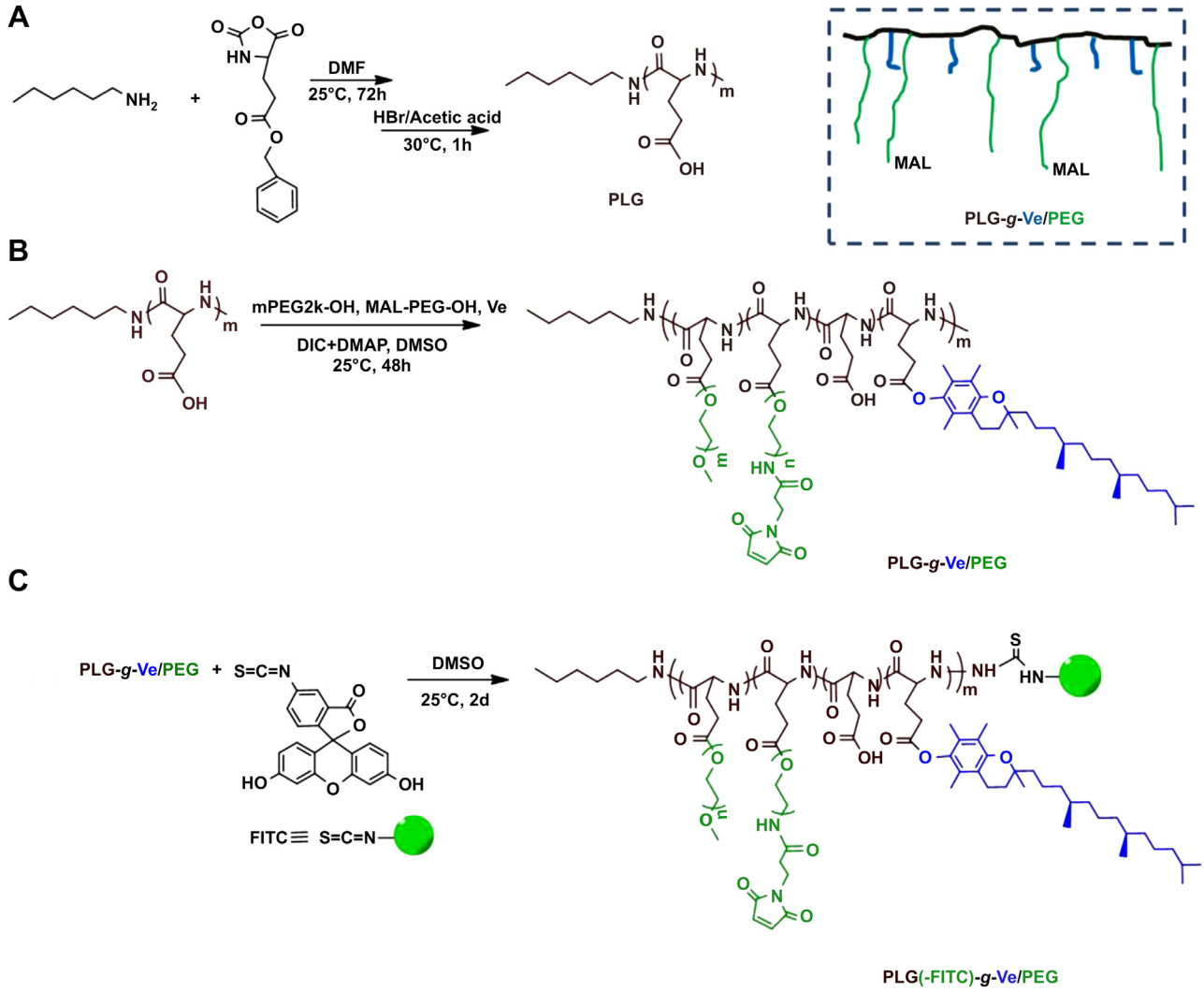

Scheme 2. Preparation of poly(L-glutamic acid) (PLG), graft copolymer (PLG-*g*-Ve/PEG), and FITC-labeled graft copolymer (PLG(-FITC)-*g*-Ve/PEG). Insets: schematic illustration of PLG-*g*-Ve/PEG.

was added. The reaction proceeded for 72 h at 25 °C and then the reaction solution was precipitated into excess ether/ethanol (2/1, v/v). The resultant poly(γ-benzyl-L-glutamate) (PBLG) was dried under vacuum for 24 h. Then 5.0 g PBLG was dissolved in 50.0 mL dichloroacetic acid and 15.0 mL HBr/acetic acid (33 wt%) was added for removing the γ-Benzyl group. After 1 h reaction at 30 °C, the solution was precipitated in excess acetone, and the final product poly(L-glutamic acid) was obtained (yield: 86.5%).

2.2.2. Synthesis of PLG-g-Ve/PEG

The graft-copolymer was prepared by condensation reaction of PLG, PEG and α-tocopherol with the condensation agents N,N′-diisopropyl carbodiimide (DIC) and 4-dimethylamiopyridine (DMAP). In brief, PLG (2.2 g, 0.20 mmol), α-tocopherol (0.83 g, 2.0 mmol), mPEG (2.4 g, 1.2 mmol), MAL-PEG-OH (2.8 g, 0.8 mmol) were dissolved in 25.0 mL DMSO, then DIC (1.1 g, 8.4 mmol) and DMAP (54 mg, 0.44 mmol) were added into the reaction system. After 48 h under 30 °C, the solution was precipitated into excess ethyl ether, and then dialyzed in distilled water for 3 days (MWCO = 3500 Da). The final product PLG-*g*-Ve/PEG was obtained after freeze drying (yield: 86%).

2.2.3. Fluorescent labeling of the graft-copolymer

The FITC labeled graft-copolymer was prepared by stirring the PLG-*g*-Ve/PEG (0.5 g, 12.8 μmol) and FITC (10.0 mg, 25.6 μmol) in DMSO solution for 2 days. After dialysis in distilled water for 3 days (MWCO = 3500 Da) and freeze drying, the green PLG(-FITC)-*g*-Ve/PEG powders were stored in dark until use.

2.2.4. Characterization

^{1}H NMR spectra were measured on a Bruker AV 400 NMR spectrometer in trifluoroacetic acid-*d* (CF_3COOD). Number-average molecular weights, weight-average molecular weights (M_n, M_w) and molecular weight distributions (polydispersity index, PDI = M_w/M_n) were determined by gel permeation chromatography (GPC) using Waters 515 HPLC pump, with DAWN EOS 18 Angles Laser Light Scattering Instrument and OPTILAB DSP Interferometric Refractometer (Wyatt Technology) as the detector. The eluant was DMF (containing 0.01 M LiBr) with a flow rate of 1.0 mL/min, and monodisperse polystyrene as standard samples. Critical micelle concentration (CMC) was estimated by fluorescence spectroscopy using pyrene as the probe, following our previous method [29].

2.3. Preparation of c(RGDfK)-decorated dual-drug-loaded micelles

2.3.1. Drug loading

DTX and CDDP loaded micelles were prepared by a two-step method. Firstly, DTX was loaded into the micelles by nanoprecipitation method. Briefly, PLG-*g*-Ve/PEG (200.0 mg) and DTX (10.0 mg) were dissolved in 10.0 mL DMSO, and then 20.0 mL phosphate buffer (pH 7.4) was added under stirring. The mixture was stirred for another 6 h and then dialyzed against distilled water using a dialysis bag (MWCO = 3500 Da). After 5000 rpm centrifuged for 4 min, the supernatant solution was filtered through a 0.45 μm filter to gain a clarified solution, and then freeze-dried to obtain the resultant DTX-loaded powder (M(DTX)). Next, 100.0 mg DTX-loaded powder was dissolved in 10.0 mL distilled water, and 20.0 mg CDDP was added after the pH was adjusted to about 8.0. Then the mixtures were left reacted at 37 °C for 72 h. After dialyzing in distilled water (to remove unloaded CDDP), DTX and CDDP dual-drug-loaded micelle solution (M($DTX_{0.5}$/Pt)) was obtained and stored at 4 °C. The solution was concentrated to required drug concentration before use. M(Pt) was prepared following the same procedure except that there was no DTX added.

Dynamic light scattering (DLS) measurements were performed using a Wyatt-QELS instrument with a vertically polarized He–Ne laser (DAWN EOS, Wyatt

Technology) at 90° collecting optics. Zeta-potentials were measured with a Zeta Potential/BI-90 Plus particle size analyzer (Brookhaven, USA) at room temperature. Transmission electron microscopy (TEM) images were taken from JEOL JEM-1011 transmission electron microscope with an accelerating voltage of 100 kV. Concentrations of Pt and DTX were determined by inductively coupled plasma mass spectrometry (ICP-MS, Xseries II, Thermoscientific, USA) and high-performance liquid chromatography (HPLC). The HPLC system consisted of a reverse-phase C-18 column (Symmetry®), with a mobile phase of acetonitrile and water (80:20 v/v) pumped at a flow rate of 1.0 mL/min at 25 °C. 20 μL aliquot of sample was injected, and the column effluent was detected at 227 nm with an UV detector (Waters 2489). Drug loading content (DLC %) and drug loading efficiency (DLE%) were calculated following the formula below:

$$\text{DLC}\,\% = \frac{\text{weight of drug in micelles}}{\text{weight of drug} - \text{loaded micelles}} \times 100\%$$

$$\text{DLE}\,\% = \frac{\text{weight of drug in micelles}}{\text{total weight of drug for loading}} \times 100\%$$

2.3.2. c(RGDfK) decoration

10.0 mL dual-drug-loaded micelle (40.0 mg) solution was mixed with 8.0 mg c(RGDfK), and agitated overnight at 37 °C. Then the c(RGDfK) decorated micelles (cRGD-M($DTX_{0.5}$/Pt)) were obtained after dialysis in distilled water for 12 h (MWCO = 3500 Da). The c(RGDfK) peptide content of the micelles was determined by measuring the arginine content following the method described in the literature [30]. Degree of modification was defined as μmol of c(RGDfK) per mg of micelles.

2.4. In vitro cytotoxicity

The relative cytotoxicity of blank micelles and drug-loaded micelles was assessed by measuring the cell viability using the MTT assay.

HeLa cells were seeded in 96-well plates at 1.0×10^5 cells per well in 200 μL of complete Dulbecco's modified Eagle's medium (DMEM) containing 10% fetal bovine serum, supplemented with 50 U/mL penicillin and 50 U/mL streptomycin, and incubated at 37 °C in 5% CO_2 atmosphere for 24 h, followed by removing the culture medium and adding the blank micelle solutions at different concentrations. The cells were subjected to MTT assay after being incubated for another 48 h.

For the drug-loaded micelles evaluation, mouse melanoma cell line B16F1 cells were applied, following the procedure similar to the above. The cells were seeded in 96-well plates at 3.0×10^3 cells per well, and 24, 48 and 72 h incubation time were applied.

The absorbance of the solution was measured on a Bio-Rad 680 microplate reader at 492 nm. Cell viability (%) was calculated according to the following equation: viability (%) = ($A_{sample}/A_{control}$) × 100%, where A_{sample} and $A_{control}$ were the absorbances of the sample well and control well, respectively.

2.5. Cellular uptake study

The cellular uptake of M($DTX_{0.5}$/Pt) and cRGD-M($DTX_{0.5}$/Pt) was evaluated by confocal laser scanning microscopy (CLSM), flow cytometry (FACS), and ICP-MS against B16F1 cells.

2.5.1. CLSM

B16F1 cells were seeded in 6-well plates at 2.0×10^5 cells per well in 2.0 mL DMEM and cultured for 24 h, and then incubated at 37 °C for additional 1 or 3 h with FITC-labeled M($DTX_{0.5}$/Pt) and cRGD-M($DTX_{0.5}$/Pt). Then, the culture medium was removed and cells were washed with PBS thrice. Thereafter, the cells were fixed with 4% (w/v) paraformaldehyde for 30 min at 25 °C, and the cells were counterstained with 4′,6-diamidino-2-phenylindole (DAPI) for cell nuclei according to the standard protocols provided by the suppliers. CLSM images were taken through the confocal microscope (Carl Zeiss LSM 780).

2.5.2. FACS

The cells were seeded in 6-well plates at 2.0×10^5 cells per well in 2.0 mL of complete DMEM and cultured for 24 h, and then incubated at 37 °C for additional 1 or 3 h with FITC-labeled M($DTX_{0.5}$/Pt) and cRGD-M($DTX_{0.5}$/Pt). Thereafter, the culture media were removed and cells were washed with PBS thrice and treated with trypsin. Then, 0.4 mL of PBS was added to each culture well, and the solutions were centrifuged for 5 min at 3000 rpm. After removal of supernatants, the cells were resuspended in 0.3 mL of PBS. Data for 1×10^4 gated events were collected, and analysis was performed by flow cytometer (Beckman, California, USA).

2.5.3. ICP-MS

B16F1 cells were seeded in a 6-well culture plate at a density of 2.0×10^5 cells per well. After attaching for 24 h, CDDP, M($DTX_{0.5}$/Pt) and cRGD-M($DTX_{0.5}$/Pt) were added into the cultured medium respectively (30.0 μg/mL, CDDP). After incubation for 1 and 4 h at 37 °C, the medium was removed and rinsed with cold PBS thrice. The cells were trypsinized and cell numbers were counted, and then incubated with nitric acid (68%, v/v) at 70 °C for 12 h. The platinum content analysis was performed using ICP-MS.

2.6. Phamocokinetics

Wistar rats were randomly divided into three groups ($n = 3$, average weight 250 g). CDDP, M($DTX_{0.5}$/Pt), and cRGD-M($DTX_{0.5}$/Pt) were administered via tail vein (Dosage, 1.5 mg CDDP equivalent/kg body weight). At defined time periods (5 min, 0.5, 1, 4, 10 and 24 h), blood samples were collected from the orbital cavity, heparinized, and centrifuged to obtain the plasma. Plasma samples were decomposed on heating in nitric acid and the Pt contents were measured by ICP-MS, following the procedure used before [31].

2.7. Tissue distribution

Xenograft melanoma model was established by subcutaneous injection of B16F1 cells in the right flank of C57BL/6 mice. The mice were handled under protocols approved by the Lab Animal Center of Jilin University. The mice (average body weight 15 g, 6 week old) were injected subcutaneously in the armpit of right anterior limb with 0.1 mL of cell suspension containing 1.0×10^6 B16F1 cells in PBS. When the tumor volume reached 100 mm^3, the mice were divided into three groups, and CDDP, M($DTX_{0.5}$/Pt), and cRGD-M($DTX_{0.5}$/Pt) were administered via tail vein (dosage: 3.0 mg CDDP equivalent/kg body weight). At defined time periods (3 min, 1, 6, 24 and 48 h), 3 mice in each group were sacrificed, and the kidney, liver, spleen, lung, heart and tumor were excised. The organs were weighed, decomposed on heating in nitric acid, evaporated to dryness, re-dissolved, and the Pt concentration was measured by ICP-MS.

2.8. Anti-tumor efficacy

The *in vivo* anti-tumor efficacy of the drug-loaded micelles was evaluated utilizing the xenograft B16F1 melanoma xeno-implanted on C57BL/6 mice. Treatments were started 5 days after cell implantation, when tumor in the mice reached a volume of 30–70 mm^3, and this day was designated as day 0. The mice were weighed and randomly divided into 5 groups (6 mice per group): saline, M(Pt), M(DTX), M($DTX_{0.5}$/Pt), and cRGD-M($DTX_{0.5}$/Pt) (dosage: 1.5 mg DTX/kg body weight, 3.0 mg CDDP equivalent/kg body weight). The injection was carried out on day 0, 2, 4, 6, 8 via tail vein. The treatment efficacy and safety evaluation were assessed by measuring the tumor volume and body weight, respectively. Tumor volume, tumor growth rate, tumor suppression rate were calculated by the following formula:

$$\text{Tumor volume}(V_t) = a \times b^2/2$$

$$\text{Tumor growth rate}(\text{TGR},\ \%) = (V_t/V_0) \times 100\%$$

$$\text{Tumor suppression rate}(\text{TSR},\ \%) = [(\text{TGR}_c - \text{TGR}_x)/\text{TGR}_c] \times 100\%$$

a, *b* are the major and minor axes of the tumors measured by caliper, V_0 represented the initial volume. c represented the control group, while x represented the treatment group.

2.9. Efficacy in treating melanoma metastasis

For the melanoma pulmonary metastatic model, C57BL/6 mice were injected intravenously through tail vein with 100 μL of B16F10 cell suspension containing 1.0×10^5 B16F10 cells, and this day was designated as day 0. At day 10, mice were randomly divided into three groups (3 animal each), saline, M($DTX_{0.5}$/Pt), and cRGD-M($DTX_{0.5}$/Pt) (dosage: 1.5 mg DTX/kg body weight, 3.0 mg CDDP equivalent/kg body weight) were injected via tail vein. The mice were sacrificed at day 20 and the lungs were removed and photographed, and the tumor colonies on the surface of lung were counted to evaluate the anti-metastasis efficacy.

2.10. Statistics

All experiments were performed at least three times and expressed as means ± SD. Data were analyzed for statistical significance using Student's *t*-test. $P < 0.05$ was considered statistically significant.

3. Results and discussion

3.1. Preparation of graft-copolymer PLG-g-Ve/PEG

Poly (L-glutamic acid) (PLG) is a kind of biodegradable polypeptide widely used in biomedical fields. Besides biodegradation, good water solubility and non-toxicity, abundant carboxyl groups in PLG could be applied for graft-modification, and further use in wide range of applications [32,33]. In this work, we firstly prepared PLG by ring opening polymerization of BLG-NCA, then hydrophobic α-tocopherol and hydrophilic PEG were grafted on to the side

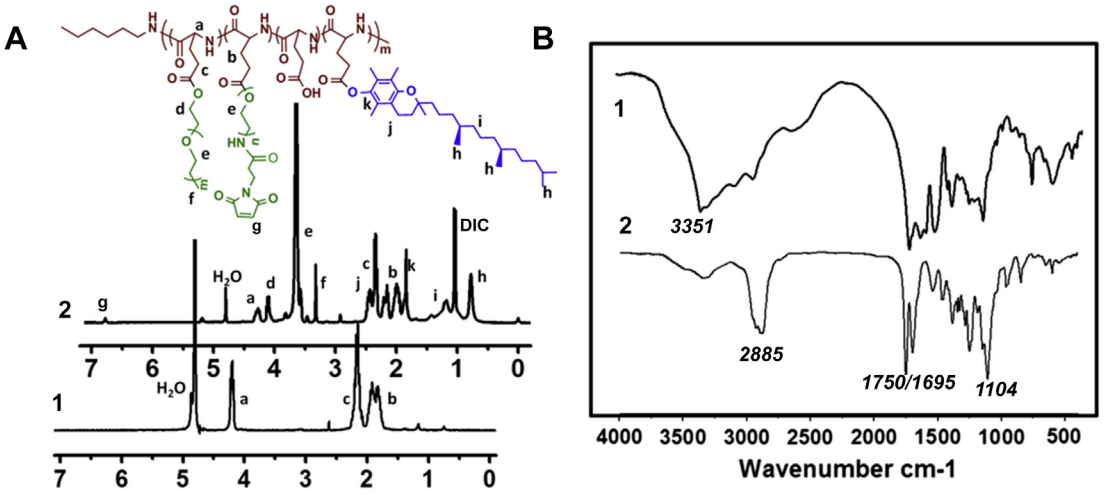

Fig. 1. ^{1}H NMR (A, in CF_3COOD), IR (B) characterization of PLG (1) and PLG-*g*-Ve/PEG (2). Molecular weight and distribution are summarized in Table 1.

chains of the PLG by condensation reaction. α-Tocopherol is a kind of chemical compound belongs to the vitamin E family. It's the most important fat-soluble antioxidants in the body [34]. Herein, α-tocopherol was applied as the hydrophobic segment for inducing self-assemble of the graft copolymer. PEG is the most widely applied polymer for reducing non-specific interaction in blood and prolonging the circulation time. Therefore, PEG was grafted to PLG as the hydrophilic segment. Besides, MAL-PEG-OH was also grafted to the backbone for further c(RGDfK) decoration.

Fig. 1 shows the ^{1}H NMR and IR spectra of PLG and PLG-*g*-Ve/PEG. In the ^{1}H NMR spectra, the resonances at δ 4.3 ppm, 2.2 and 2.0–1.8 ppm were assigned to the protons of the poly (L-glutamic acid) backbone (–C(O)C***H***(CH_2–)NH–) and the methylene protons of glutamic acid (–CH–C***H***$_2$–C***H***$_2$–CO–) residues. The number of repeating units could be calculated by the integral area of peaks at δ 4.3 ppm and 0.75 ppm which belongs to the methyl of *n*-hexylamine (–C***H***$_3$). In the ^{1}H NMR of PLG-*g*-Ve/PEG, the newly appeared resonances at δ 0.75 ppm and 3.65 ppm were attributed to the protons of methyl and methylene in α-tocopherol and PEG, respectively. The graft ratio was calculated by the integral ratio with protons in PLG. For IR spectra, the broad vibration absorption between 3000 and 3500 cm^{-1} belongs to the OH of the carboxylic acid groups. In the IR spectrum of PLG-*g*-Ve/PEG, the strong absorption at 1104 and 2885 cm^{-1} was attributed to the stretching vibration of methylene in PEG, and the absorption peak at 1750 cm^{-1} belongs to the carboxylic ether, a little different from the carboxylic acid at 1695 cm^{-1}. Detailed characterization of PLG-*g*-Ve/PEG was listed in Table 1.

3.2. Self-assembly, drug-loading and c(RGDfK)-decoration

After the simultaneous modification of hydrophilic PEG and hydrophobic α-tocopherol, the graft-copolymer could self-assemble into micelles in water. PLG-*g*-Ve/PEG blank micelles were prepared by nanoprecipitation method. The hydrodynamic radius R_h of the micelles was 44 ± 13 nm. TEM showed the uniform spherical structure. The critical micelle concentration (CMC) of the blank micelles was measured by the pyrene fluorescence probe method. As shown in Fig. 2, the fluorescence excitation spectrum of pyrene had a blue shift from 339 nm to 335 nm when the micelle concentration decreased from 0.5 mg/mL. This was caused by the transition of pyrene molecule from non-polar micelle core to the polar solvent. The intensity ratios of I_{339}/I_{335} were plotted as a function of logarithm of polymer concentration, and CMC was corresponding to the turning point concentration, 1.9×10^{-3} mg/mL.

The PLG-*g*-Ve/PEG graft-copolymer was applied for co-encapsulation of DTX and CDDP. A two-step method was applied. Firstly, DTX was loaded into the hydrophobic core of the micelles by nanoprecipitation method, the drug loading content (DLC%) and efficiency (DLE%) of the single-DTX loaded micelles (M(DTX)) were 4.3% and 90.3%, measured by HPLC. Then M(DTX) was re-dissolved in water, CDDP was loaded to the residual glutamic acid groups, and the dual-drug-loaded micelles M($DTX_{0.5}$/Pt) were obtained. The DLC% and DLE% of CDDP were 8.5% and 50.9%, measured by ICP-MS. The single platinum loaded micelles (M(Pt)) were prepared by similar method except no DTX was added, with DLC% of CDDP 8.7%. c(RGDfK) decorated dual-drug-loaded micelles cRGD-M($DTX_{0.5}$/Pt) were prepared by Michael addition reaction of the sulfhydryl group in c(RGDfK) with the maleimide in MAL-PEG- of the M($DTX_{0.5}$/Pt). The morphology, size and zeta-potential of the drug-loaded micelles were listed in Fig. 2 and Table 2. All the micelles were spherical with moderate size and negative surface charge. After CDDP chelation, the hydrodynamic radius R_h decreased from 45 nm to smaller than 26 nm, while zeta potential became less negative from −35.8 to −15.3 mV. This could be explained by the consumption of the carboxyl groups due to Pt^{II} chelation. c(RGDfK) decoration did not have an obvious effect on the size, while the surface potential of micelles was further increased to −8.1 mV. The peptide content on the surface was determined by measuring

Table 1
Characterization of PLG-*g*-Ve/PEG.

Entry	DP of PLG[a]	Grafting molar content of PEG and MAL-PEG[a]	Grafting molar content of Ve[a]	$M_n/10^4$ (g mol^{-1})[a]	$M_n/10^4$ (g mol^{-1})[b]	PDI[b]
PLG-*g*-Ve/PEG	85	6 + 4	10	3.9	4.7	1.4

[a] Measured by ^{1}H NMR.
[b] Measured by GPC.

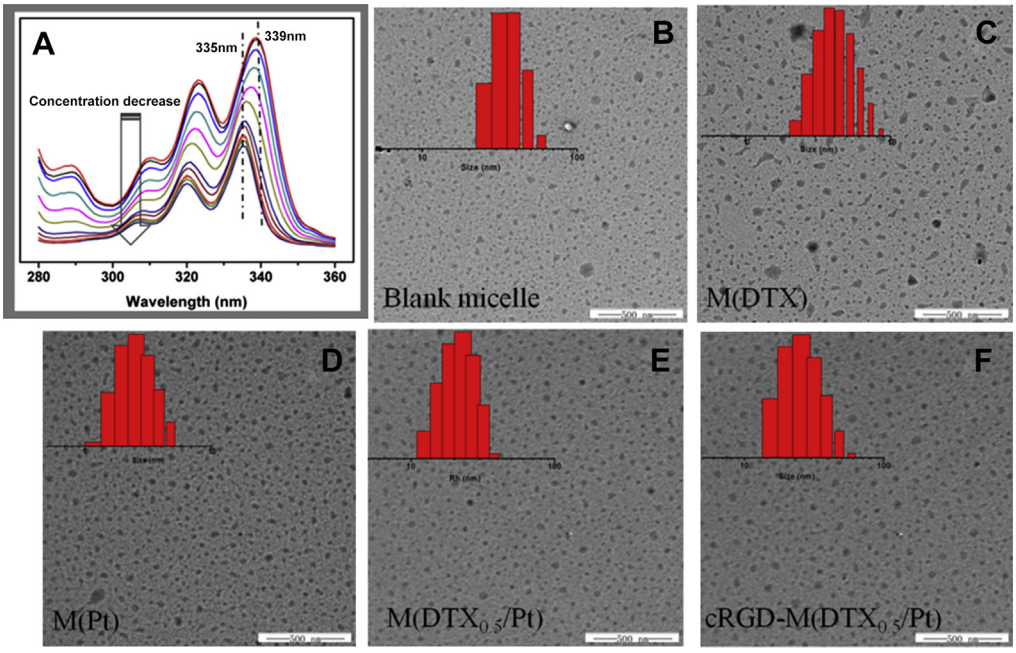

Fig. 2. Characterization of the blank micelles and the drug-loaded micelles. A. Fluorescence spectrum of pyrene in the blank micelles by dilution of stock solution from 0.5 g/L to 2.4×10^{-4} g/L. A blue shift takes place and the critical micelle concentration (CMC) was determined as 1.9×10^{-3} g/L. B–F are the DLS and TEM results of the blank micelles and the drug-loaded micelles, and the hydrodynamic radius and zeta potentials are summarized in Table 2.

arginine using a fluorimetric assay. The reagent 9,10-phenanthrenequinone was mixed with the sample at a high pH followed by acidification to convert arginine residues to a strongly fluorescent small molecule (λ_{ex} = 312, λ_{em} = 340–570 nm). The amount of c(RGDfK) on the surface was 0.15 μmol/mg drug-loaded micelles.

3.3. Synergistic cytotoxicity

As a potential drug carrier, the cyto-compatibility of the graft-copolymer was evaluated by MTT assay with HeLa cells. Fig. 3 showed the cell viability of HeLa cells when incubated with PLG-*g*-Ve/PEG and PEI 25k for 48 h. The graft-copolymer showed good biocompatibility, since over 80% of survival rate was observed at a concentration even to 500 μg/mL, while PEI 25k showed obvious cell proliferation inhibition effect.

DTX is a representative microtubule-stabilizing chemotherapy drug, and CDDP is one of the most widely used DNA-modifying chemotherapy drugs. The combination of DTX and CDDP is expected to have good synergism effect against wide range of cancer cell lines due to the different action mechanism [35–37]. c(RGDfK), a cyclic peptide developed by Kessler and co-workers [38], is a highly specific ligand targeting the $\alpha_v\beta_3$ integrin, which is overexpressed in various tumor vascular endothelial cells and some specific tumor cells [39–41]. Herein, B16F1 melanoma cells were applied to test the synergistic toxicity of the co-loaded two drugs and the enhanced toxicity after c(RGDfK) decoration. The survival rate histogram of B16F1 cells after incubation with M(Pt), M(DTX), M(DTX$_{0.5}$/Pt) and cRGD-M(DTX$_{0.5}$/Pt) at 24, 48, 72 h was shown in Fig. 3. All the micelles showed time and concentration dependent tumor cell proliferation inhibition effect. At 72 h, the IC_{50} values of M(Pt), M(DTX), M(DTX$_{0.5}$/Pt) and cRGD-M(DTX$_{0.5}$/Pt) are 6.36 μg/mL (CDDP), >5 μg/mL(DTX), 2.49 μg/mL(DTX) and 1.54 μg/mL(DTX). Dual-drug-loaded micelles showed synergistic effect since better proliferation inhibition effect over single-drug-loaded micelles. After c(RGDfK) decoration, the effect was further enhanced, and IC_{50} values further decreased.

3.4. Enhanced endocytosis of cRGD-M(DTX$_{0.5}$/Pt)

The enhanced tumor cell proliferation inhibition effect of c(RGDfK) decorated micelles might be attributed to the enhanced uptake rate promoted by the receptor mediated endocytosis. To clarify this, PLG(-FITC)-*g*-Ve/PEG was used to prepare the drug-loaded or c(RGDfK)-decorated micelles. The endocytosis rate was measured by CLSM and FACS. Pt in micelles was applied as the interior label for measuring the micelle uptake by ICP-MS.

As shown in Fig. 4, M(DTX$_{0.5}$/Pt) and cRGD-M(DTX$_{0.5}$/Pt) could both be effectively uptake by B16F1 cells, and as time prolonged, more micelles endocytosed. The c(RGDfK)-decorated micelles showed faster tumor cell uptake rate as much stronger signal was seen in the CLSM image. This was consistent with the FACS results. Stronger mean fluorescent signal was observed in the treatment with cRGD-M(DTX$_{0.5}$/Pt) than M(DTX$_{0.5}$/Pt). For ICP-MS results, free CDDP diffused quickly into B16F1 cells, while loaded cisplatin showed slower uptake rate than free CDDP. This may be ascribed to the negative charge of the micelles, which blocked the fusion with the negative cell membrane whereas the negative surface charge was helpful during blood circulation for reducing non-specific protein absorption. c(RGDfK) decoration solved the embarrassment. Five times increases in intracellular Pt concentration were

Table 2
Hydrodynamic radius (R_h) and zeta-potential of the micelles.

	Blank micelle	M(DTX)	M(Pt)	M(DTX$_{0.5}$/Pt)	cRGD-M(DTX$_{0.5}$/Pt)
R_h (nm)	44 ± 13	45 ± 20	23 ± 4	26 ± 11	28 ± 9
Zeta potential (mV)	−34.0 ± 8.2	−35.8 ± 3.9	−14.9 ± 2.4	−15.3 ± 1.2	−8.1 ± 3.0

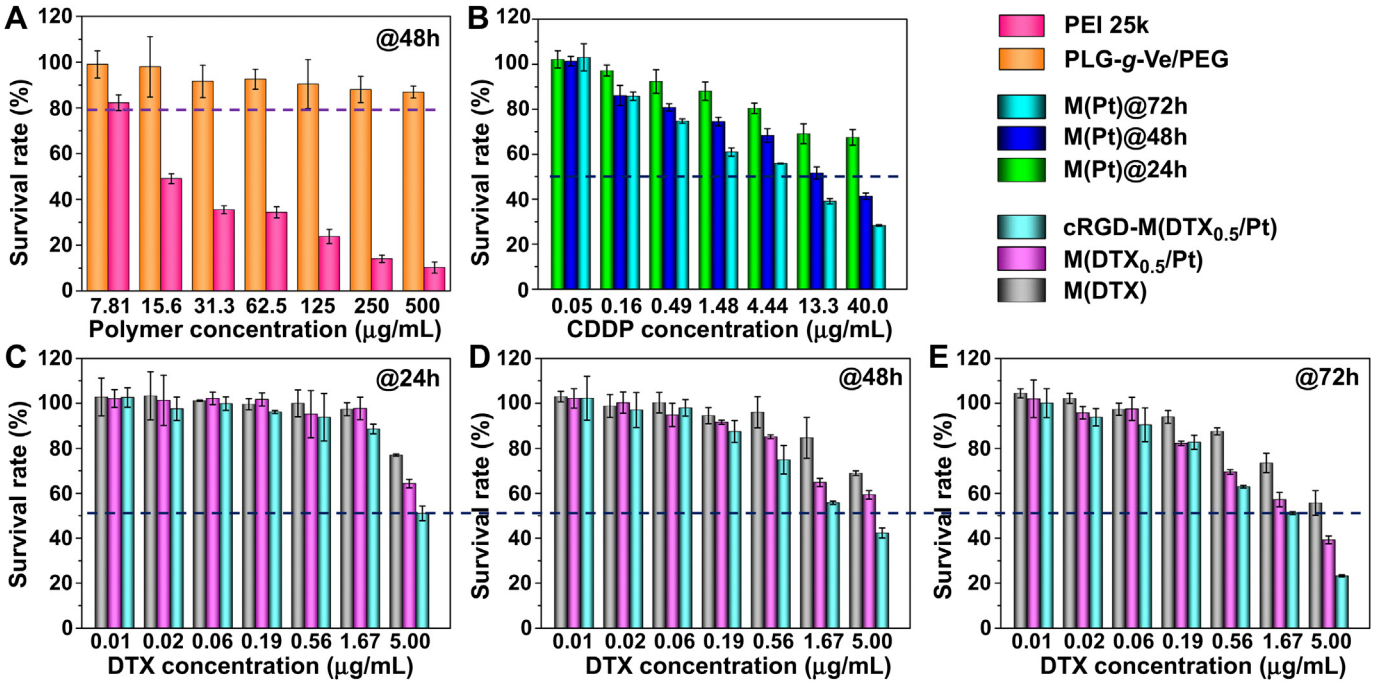

Fig. 3. MTT results. A is the survival rate of HeLa cells after incubation with PEI 25k and PLG-*g*-Ve/PEG for 48 h. B is the survival rates of B16F1 cells after incubation with M(Pt) micelles for 24, 48 and 72 h. C-E are the survival rates of M(DTX), M($DTX_{0.5}$/Pt) and cRGD-M($DTX_{0.5}$/Pt) after incubation with B16F1 cells for 24, 48 and 72 h. All the results are average of three measurements, and list as mean ± SD.

observed after c(RGDfK) decoration of the micelles. The above results indicate that c(RGDfK) would enhance the endocytosis of the drug-loaded micelles, therefore, would result in enhanced tumor cell proliferation inhibition effect.

3.5. Pharmacokinetics and tissue accumulation

To further clarify the performance of the c(RGDfK) targeting ligands *in vivo*, we tested the metabolic behavior of the micelles with or without c(RGDfK) decoration in blood, organs and tumors. As stated above, chelated platinum could be applied as the marker for the *in vivo* fate of the micelles, and free CDDP was administered as control.

The metabolic behavior in blood (pharmacokinetics) was studied in Wistar rats. CDDP, M($DTX_{0.5}$/Pt) or cRGD-M($DTX_{0.5}$/Pt) was injected via tail vein (1.5 mg/kg, CDDP basis). Pt concentrations were measured by ICP-MS. As shown in Fig. 5, CDDP was quickly cleared from blood after intravenous administration, and the Pt

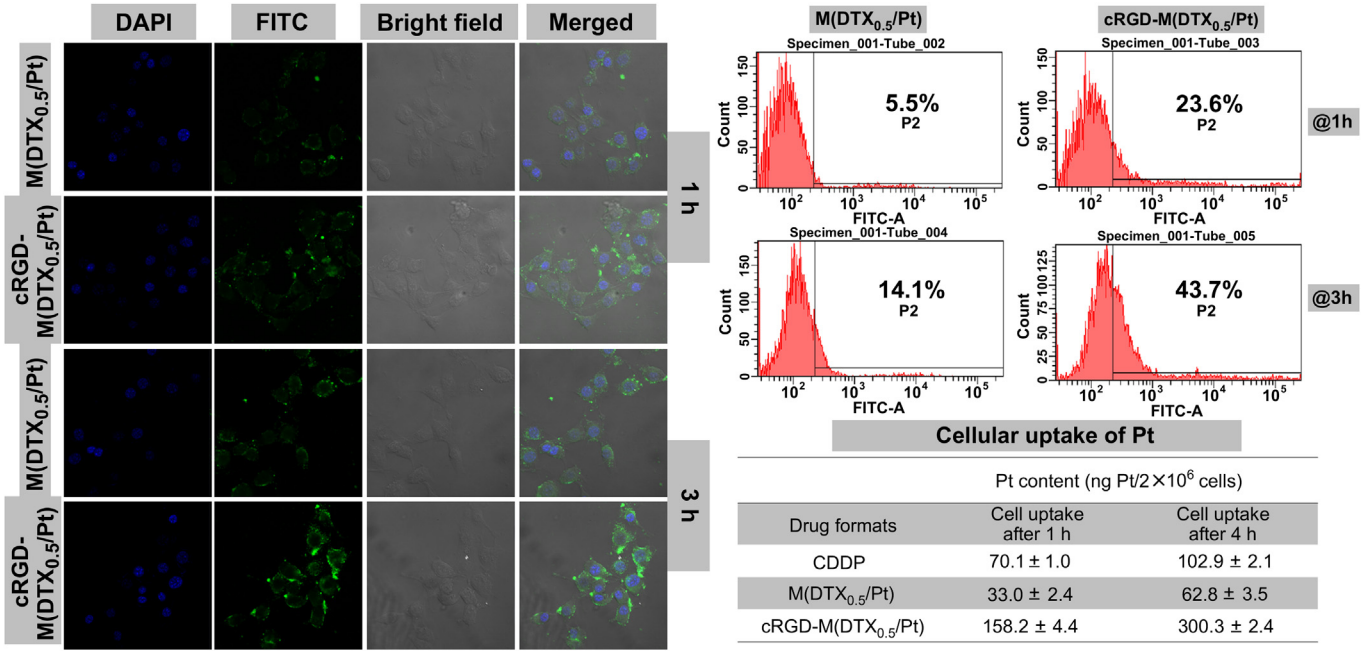

Pt content (ng Pt/2×10^6 cells)

Drug formats	Cell uptake after 1 h	Cell uptake after 4 h
CDDP	70.1 ± 1.0	102.9 ± 2.1
M($DTX_{0.5}$/Pt)	33.0 ± 2.4	62.8 ± 3.5
cRGD-M($DTX_{0.5}$/Pt)	158.2 ± 4.4	300.3 ± 2.4

Fig. 4. Cellular uptake studies of M($DTX_{0.5}$/Pt) and cRGD-M($DTX_{0.5}$/Pt) calculated by CLSM, FACS and ICP-MS.

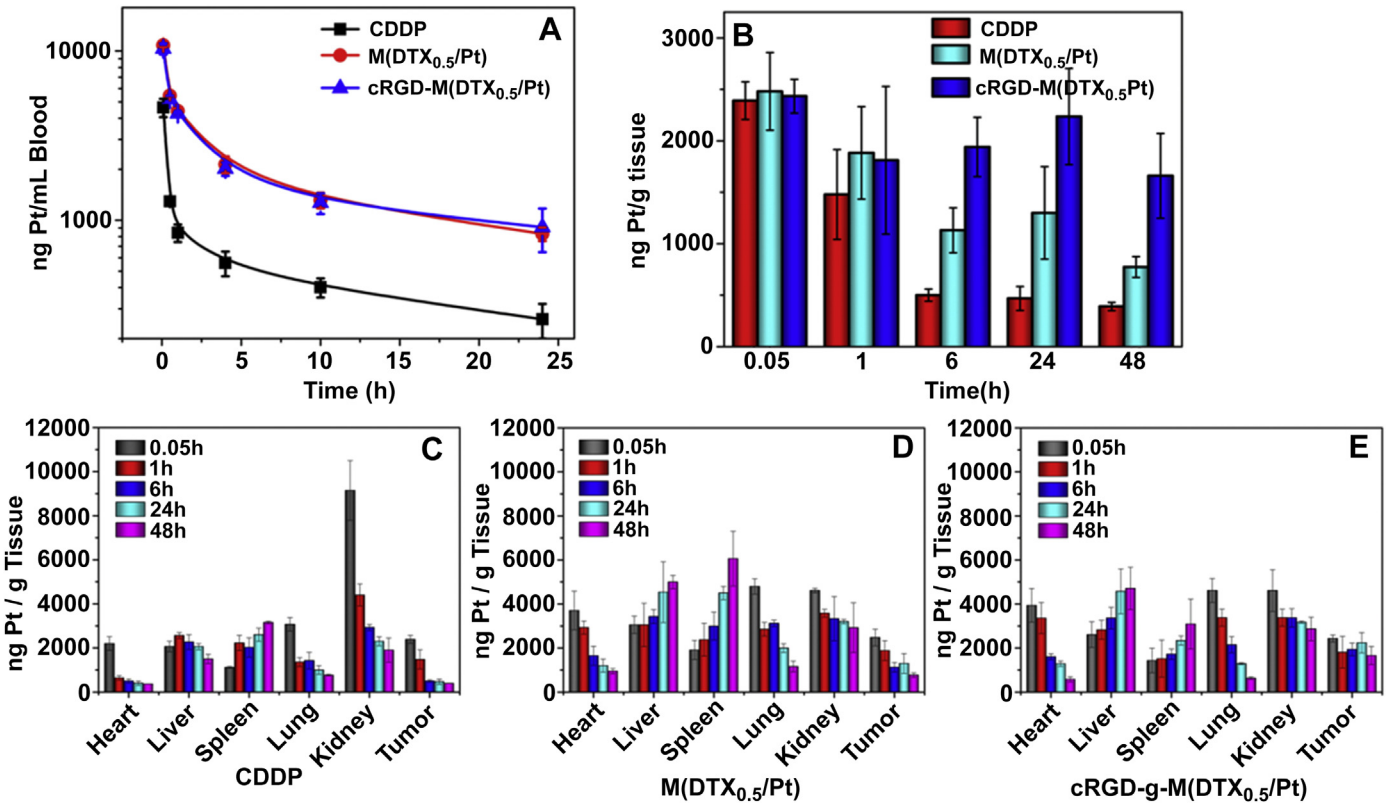

Fig. 5. Phamacokinetics (A), tissue (C–E) and tumor (B) metabolism of CDDP, M($DTX_{0.5}$/Pt) and cRGD-M($DTX_{0.5}$/Pt). The phamacokinetics was carried out on healthy Wistar rats, at a dosage of 1.5 mg CDDP equivalent/kg body weight, blood samples were collected at 5 min, 0.5, 1, 4, 10 and 24 h. Tissue and tumor distribution was carried out on B16F1 melanoma xenograft-bearing C57BL/6 mice at a dosage of 3.0 mg CDDP equivalent/kg body weight. The drug concentration was measured according to the Pt interior marker by ICP-MS. Each group was expressed as mean ± SD ($n = 3$).

concentration decreased to less than 550 ng/mL blood in 4 h. Micelles loaded with Pt showed significantly prolonged blood circulation time, and the Pt concentration remained over 1000 ng/mL blood after 24 h c(RGDfK) decoration showed no obvious effect on blood circulation in healthy rats. The significant prolonged blood circulation time of M($DTX_{0.5}$/Pt) and cRGD-M($DTX_{0.5}$/Pt) indicated that the micelle systems could protect the loaded drugs from direct interaction with plasma proteins, and escaping the reticuloendothelial system (RES) uptake and renal clearance. This enhanced the possibility for passive accumulation of the micelles in tumor tissue by enhanced permeability and retention (EPR) effect.

The distribution and metabolic behavior of the drug-loaded micelles in organs and tumors were studied in C57BL/6 mice bearing xenograft B16F1 melanoma. Pt was used as the interior label for following the route of the micelles. When tumor volume reached 100 mm^3, CDDP, M($DTX_{0.5}$/Pt) or cRGD-M($DTX_{0.5}$/Pt) was injected via tail vein (3.0 mg/kg, CDDP). Kidney, liver, spleen, lung, heart and tumor were excised at defined time intervals. The Pt content was measured by ICP-MS after treating by nitric acid. As shown in Fig. 5, free CDDP quickly diffused into and cleared out from each organ, while a significant fast and high distribution was observed in the kidney. Because nephrotoxicity of CDDP is dependent on the maximum urinary Pt concentration and on the peak Pt concentration in the kidney tubules, the high peak concentration of Pt in the kidney induced the severe nephrotoxicity of CDDP [42]. In contrast, the drugs loaded in micelles showed well distribution in each organ, and no acute spread in kidney was observed. This reflected the different *in vivo* fate of free drugs and drugs loaded in micelles. Free drugs quickly spread to each organ and then cleared out or interact with biological systems, while drugs loaded in micelles were protected from premature interacting with physiological environment, and had long blood half-life.

Next, we compared the metabolism of CDDP, M($DTX_{0.5}$/Pt) and cRGD-M($DTX_{0.5}$/Pt) in tumor tissue in 48 h. In the initial 3 min, free drugs and loaded drugs quickly entered the tumor tissue. After that, free drugs diffused out, and the drug concentration quickly decreased. While for the loaded drugs, obvious retention effect was seen, especially for the c(RGDfK) decorated micelles. After 6 h, the concentration of Pt in cRGD-M($DTX_{0.5}$/Pt) group was almost double as compared to M($DTX_{0.5}$/Pt) while quarter as compared to free CDDP. These results demonstrated that the drug-loaded micelles would quickly diffuse into tumors after injection, and would keep high drug concentrations in tumor tissues due to the EPR effect. While after c(RGDfK) decoration, this effect was enhanced due to the interaction of c(RGDfK) with the integrin over-expressed on the tumor cell surfaces.

3.6. *In vivo anti-tumor and anti-metastasis efficacy*

The *in vivo* anti-tumor efficacy was tested on the xenograft B16F1 melanoma established on C57BL/6 mice. When tumor volume grown to 30–70 mm^3, mice were divided into five groups. Saline, M(Pt), M(DTX), M($DTX_{0.5}$/Pt), cRGD-M($DTX_{0.5}$/Pt) were injected respectively via tail vein on day 0, 2, 4, 6, 8. The tumor volume was measured and body weight was recorded for 16 days. As shown in Fig. 6, all the drug-loaded micelles showed obvious anti-tumor efficacy. The dual-drug-loaded micelles showed better anti-tumor effect than single-drug-loaded micelles due to the synergistic effect of the two drugs. The c(RGDfK) targeted dual-drug-loaded micelles resulted in the best tumor inhibition effect.

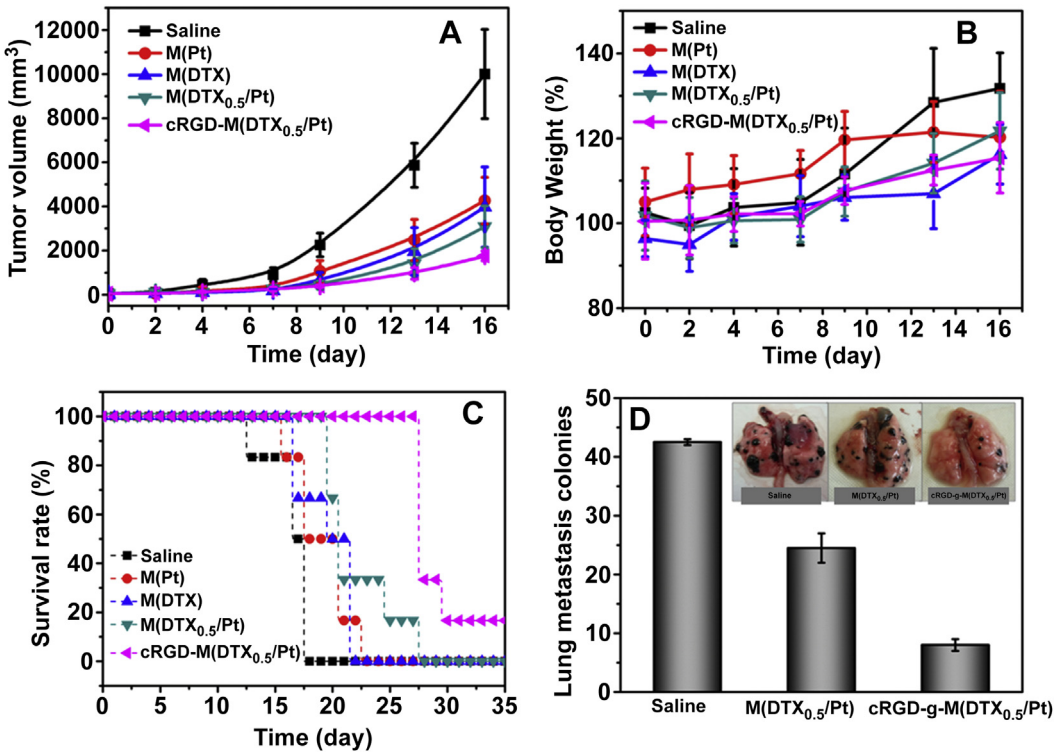

Fig. 6. *In vivo* anti-tumor and anti-metastasis efficacy of the drug-loaded micelles. A–C are the tumor volume, body weight and survival rate of the B16F1 melanoma xenograft bearing C57BL/6 mice. Saline, M(Pt), M(DTX), M($DTX_{0.5}$/Pt) and cRGD-M($DTX_{0.5}$/Pt) were administered via tail vein at dosage of 1.5 mg DTX, 3.0 mg CDDP equivalent/kg body weight on day 0, 2, 4, 6, 8 (data are mean ± SD, $n = 6$). The tumor volume, tumor growth rate (TGR%) and tumor suppression rate (TSR%) at day 16 were summarized in Table 3. For the B16F10 pulmonary metastasis (D), saline, M($DTX_{0.5}$/Pt) and cRGD-M($DTX_{0.5}$/Pt) were administered at 1.5 mg DTX, 3.0 mg CDDP equivalent/kg body weight on day 10. The lung photos (insets) and tumor colonies were recorded on day 20 (data are mean ± SD, $n = 3$).

At day 16, M(Pt), M(DTX), M($DTX_{0.5}$/Pt), cRGD-M($DTX_{0.5}$/Pt) got tumor suppression rate (TSR%) of 59.4%, 67.3%, 70.7% and 85.1%, respectively (Table 3).

Body weight change is a reflection of the system toxicity. As shown in Fig. 6, all the drug-loaded micelles showed no body weight loss during the 16 days observation period, which means no obvious toxicity. From the survival rate results of the five groups, we could see that the survival time was prolonged after treatment with the drug-loaded micelles, and the best results were still obtained from the group with cRGD-M($DTX_{0.5}$/Pt) micelles, which was consistent with the tumor inhibition results.

Metastasis is one of the most important reason for chemotherapy failure. Tumor metastases inhibition can be achieved by selective targeting of $\alpha_v\beta_3$ integrin with c(RGDfK) since $\alpha_v\beta_3$ plays an important role in tumor cell attachment, spreading and migration [43–45]. Herein, we established the melanoma pulmonary metastases model and tried our micelles on the inhibition of the metastases.

The melanoma pulmonary metastases model was established by injection of 1.0×10^5 B16F10 cells via tail vein [46,47]. After 10 days, saline, M($DTX_{0.5}$/Pt) and cRGD-M($DTX_{0.5}$/Pt) were administrated via tail vein. At day 20, the lung was excised and photographed. Tumor colonies on the lung surface were counted. As shown in Fig. 6, the targeted dual-drug-loaded micelles showed obvious inhibition effect on the melanoma metastasis to lung. Therefore, the cRGD-M($DTX_{0.5}$/Pt) micelles showed great potential in melanoma chemotherapy, and in other solid or metastasis tumors.

4. Conclusion

A targeted dual-drug-loaded micelle system was developed for enhanced anti-cancer efficacy. The enhanced anti-cancer efficacy of the loaded drugs can be connected with long circulation time, enhanced accumulation and retention in tumor tissue, quickly endocytosis, and synergistic cytotoxicity. Polypeptide-based PLG-*g*-Ve/PEG graft copolymer was prepared by condensation reaction of poly(L-glutamic acid) with PEG and α-tocopherol. DTX and CDDP were co-loaded inside the micelles by hydrophobic and chelation effect. c(RGDfK) was decorated on the surface for $\alpha_v\beta_3$ integrin targeting. The co-loaded drugs showed synergistic cytotoxicity to inhibit tumor cell proliferation. c(RGDfK) decoration considerably enhanced the endocytosis rate and retention effect of the micelles in tumor tissue. Therefore, the micelle system showed good anti-tumor and anti-metastasis efficacy in melanoma bearing mice.

Table 3
Tumor volume, TGR%, and TSR% of the treatment groups.

	Saline	M(Pt)	M(DTX)	M($DTX_{0.5}$/Pt)	cRGD-M($DTX_{0.5}$/Pt)
Tumor volume@Day0, V_0	60.0(±11.6)	63.1(±10.7)	72.8(±16.2)	63.1(±10.7)	70.5(±13.2)
Tumor volume@Day16, V_t	10,008(±2027)	4268(±1060)	3974(±1819)	3079(±953)	1756(±219)
TGR%@Day16	16,680	6764	5459	4880	2491
TSR%@Day16	–	59.4	67.3	70.7	85.1

Acknowledgments

This research was financially supported by National Natural Science Foundation of China (Projects 51173184, 51233004, 51021003, 21074018, 51373168 and 51390484), Ministry of Science and Technology of China (International Cooperation and Communication Program 2011DFR51090), and the Program of Scientific Development of Jilin Province (20130206066GX, 20130727050YY).

Dr. Zaheer Ahmad (saubanzaheer@gmail.com, Department of Chemistry, Quaid-I-Azam University, Pakistan) is appreciated for polishing English.

References

[1] Cabral H, Nishiyama N, Kataoka K. Supramolecular nanodevices: from design validation to theranostic nanomedicine. Acc Chem Res. 2011;44:999–1008.
[2] Alexis F, Pridgen EM, Langer R, Farokhzad OC. Nanoparticle technologies for cancer therapy. In: Schäfer-Korting M, editor. Drug delivery. Berlin, Heidelberg: Springer; 2010. pp. 55–86.
[3] Nishiyama N, Okazaki S, Cabral H, Miyamoto M, Kato Y, Sugiyama Y, et al. Novel cisplatin-incorporated polymeric micelles can eradicate solid tumors in mice. Cancer Res. 2003;63:8977–83.
[4] Li MQ, Song WT, Tang ZH, Lv SX, Lin L, Sun H, et al. Nanoscaled poly(L-glutamic acid)/doxorubicin-amphiphile complex as pH-responsive drug delivery system for effective treatment of nonsmall cell lung cancer. ACS Appl Mater Interfaces 2013;5:1781–92.
[5] Maeda H. Tumor-selective delivery of macromolecular drugs via the EPR effect: background and future prospects. Bioconjug Chem 2010;21:797–802.
[6] Gabizon AA. Stealth liposomes and tumor targeting: one step further in the quest for the magic bullet. Clin Cancer Res 2001;7:223–5.
[7] Ibrahim NK, Desai N, Legha S, Soon-Shiong P, Theriault RL, Rivera E, et al. Phase I and pharmacokinetic study of ABI-007, a Cremophor-free, protein-stabilized, nanoparticle formulation of paclitaxel. Clin Cancer Res 2002;8:1038–44.
[8] Lee KS, Chung HC, Im SA, Park YH, Kim CS, Kim SB, et al. Multicenter phase II trial of Genexol-PM, a Cremophor-free, polymeric micelle formulation of paclitaxel, in patients with metastatic breast cancer. Breast Cancer Res Treat 2008;108:241–50.
[9] Matsumura Y, Kataoka K. Preclinical and clinical studies of anticancer agent-incorporating polymer micelles. Cancer Sci. 2009;100:572–9.
[10] Satchi-Fainaro R, Puder M, Davies JW, Tran HT, Sampson DA, Greene AK, et al. Targeting angiogenesis with a conjugate of HPMA copolymer and TNP-470. Nat Med 2004;10:255–61.
[11] Florence AT. Pharmaceutical nanotechnology: more than size ten topics for research. Int J Pharm 2007;339:1–2.
[12] Bae YH, Park K. Targeted drug delivery to tumors: myths, reality and possibility. J Control Release 2011;153:198–205.
[13] Osada K, Kataoka K. Drug and gene delivery based on supramolecular assembly of PEG-polypeptide hybrid block copolymers. Adv Polym Sci 2006;202:113–53.
[14] Laginha KM, Verwoert S, Charrois GJR, Allen TM. Determination of doxorubicin levels in whole tumor and tumor nuclei in murine breast cancer tumors. Clin Cancer Res 2005;11:6944–9.
[15] Hong RL, Huang CJ, Tseng YL, Pang VF, Chen ST, Liu JJ, et al. Direct comparison of liposomal doxorubicin with or without polyethylene glycol coating in C-26 tumor-bearing mice: is surface coating with polyethylene glycol beneficial? Clin Cancer Res 1999;5:3645–52.
[16] Tsukioka Y, Matsumura Y, Hamaguchi T, Koike H, Moriyasu F, Kakizoe T. Pharmaceutical and biomedical differences between micellar doxorubicin (NK911) and liposomal doxorubicin (Doxil). Jpn J Cancer Res. 2002;93:1145–53.
[17] Dong XW, Mumper RJ. Nanomedicinal strategies to treat multidrug-resistant tumors: current progress. Nanomedicine (Lond) 2010;5:597–615.
[18] Szakacs G, Paterson JK, Ludwig JA, Booth-Genthe C, Gottesman MM. Targeting multidrug resistance in cancer. Nat Rev Drug Discov 2006;5:219–34.
[19] Peer D, Karp JM, Hong S, Farokhzad OC, Margalit R, Langer R. Nanocarriers as an emerging platform for cancer therapy. Nat Nanotechnol 2007;2:751–60.
[20] Hrkach J, Von Hoff D, Ali MM, Andrianova E, Auer J, Campbell T, et al. Preclinical development and clinical translation of a PSMA-targeted docetaxel nanoparticle with a differentiated pharmacological profile. Sci Transl Med 2012;4:128–39.
[21] Postmus PE. Cisplatin and paclitaxel for non-small-cell lung cancer: the European experience. Oncology 1999;13:26–9.
[22] Soma CE, Dubernet C, Bentolila D, Benita S, Couvreur P. Reversion of multidrug resistance by co-encapsulation of doxorubicin and cyclosporin A in polyalkylcyanoacrylate nanoparticles. Biomaterials 2000;21:1–7.
[23] Liu T, Zhang Y-f, Liu S-y. Drug and plasmid DNA co-delivery nanocarriers based on abctype polypeptide hybrid miktoarm star copolymers. Chin J Polym Sci 2013;31:924–37.
[24] Hu CM, Aryal S, Zhang L. Nanoparticle-assisted combination therapies for effective cancer treatment. Ther Deliv 2010;1:323–34.
[25] Xiao H, Li W, Qi R, Yan L, Wang R, Liu S, et al. Co-delivery of daunomycin and oxaliplatin by biodegradable polymers for safer and more efficacious combination therapy. J Control Release 2012;163:304–14.
[26] Chen LN, Wang Y, Zhu Y, Sun YX, Wang YX. Stimulus-responsive polyplexes with drug and gene co-delivery. Chem J Chin Univ-Chin 2013;34:720–5.
[27] Kolishetti N, Dhar S, Valencia PM, Lin LQ, Karnik R, Lippard SJ, et al. Engineering of self-assembled nanoparticle platform for precisely controlled combination drug therapy. Proc Natl Acad Sci U S A 2010;107:17939–44.
[28] Tian HY, Deng C, Lin H, Sun JR, Deng MX, Chen XS, et al. Biodegradable cationic PEG-PEI-PBLG hyperbranched block copolymer: synthesis and micelle characterization. Biomaterials 2005;26:4209–17.
[29] Song WT, Tang ZH, Li MQ, Lv SX, Yu HY, Ma LL, et al. Tunable pH-sensitive poly(beta-amino ester)s synthesized from primary amines and diacrylates for intracellular drug delivery. Macromol Biosci 2012;12:1375–83.
[30] Graf N, Bielenberg DR, Kolishetti N, Muus C, Banyard J, Farokhzad OC, et al. αVβ3 Integrin-targeted PLGA-PEG nanoparticles for enhanced anti-tumor efficacy of a Pt(IV) prodrug. ACS Nano 2012;6:4530–9.
[31] Song WT, Li MQ, Tang ZH, Li QS, Yang Y, Liu HY, et al. Methoxypoly(ethylene glycol)-block-poly(L-glutamic acid)-loaded cisplatin and a combination with iRGD for the treatment of non-small-cell lung cancers. Macromol Biosci 2012;12:1514–23.
[32] Deming TJ. Synthetic polypeptides for biomedical applications. Prog Polym Sci 2007;32:858–75.
[33] He C, Zhuang X, Tang Z, Tian H, Chen X. Stimuli-sensitive synthetic polypeptide-based materials for drug and gene delivery. Adv Healthcare Mater 2012;1:48–78.
[34] Tao YH, Han JF, Dou HY. Paclitaxel-loaded tocopheryl succinate-conjugated chitosan oligosaccharide nanoparticles for synergistic chemotherapy. J Mater Chem 2012;22:8930–7.
[35] Vasey PA, Paul J, Birt A, Junor EJ, Reed NS, Symonds RP, et al. Docetaxel and cisplatin in combination as first-line chemotherapy for advanced epithelial ovarian cancer. J Clin Oncol 1999;17:2069–80.
[36] Le Chevalier T, Berille J, Zalcberg JR, Millward MJ, Monnier A, Douillard JY, et al. Overview of docetaxel (Taxotere)/cisplatin combination in non-small cell lung cancer. Semin Oncol 1999;26:13–8.
[37] Roth AD, Maibach R, Martinelli G, Fazio N, Aapro MS, Pagani O, et al. Docetaxel (Taxotere (R))–cisplatin (TC): an effective drug combination in gastric carcinoma. Ann Oncol 2000;11:301–6.
[38] Haubner R, Gratias R, Diefenbach B, Goodman SL, Jonczyk A, Kessler H. Structural and functional aspects of RGD-containing cyclic pentapeptides as highly potent and selective integrin $\alpha_V\beta_3$ antagonists. J Am Chem Soc. 1996;118:7461–72.
[39] Yang T, Wang Y, Li Z, Dai W, Yin J, Liang L, et al. Targeted delivery of a combination therapy consisting of combretastatin A4 and low-dose doxorubicin against tumor neovasculature. Nanomedicine 2012;8:81–92.
[40] Eldar-Boock A, Miller K, Sanchis J, Lupu R, Vicent MJ, Satchi-Fainaro R. Integrin-assisted drug delivery of nano-scaled polymer therapeutics bearing paclitaxel. Biomaterials 2011;32:3862–74.
[41] Tian HY, Lin L, Chen J, Chen XS, Park TG, Maruyama A. RGD targeting hyaluronic acid coating system for PEI-PBLG polycation gene carriers. J Control Release 2011;155:47–53.
[42] Levi FA, Hrushesky WJM, Halberg F, Langevin TR, Haus E, Kennedy BJ. Lethal nephrotoxicity and hematologic toxicity of cis-diamminedichloroplatinum ameliorated by optimal circadian timing and hydration. Eur J Cancer Clin Oncol 1982;18:471–7.
[43] Desgrosellier JS, Cheresh DA. Integrins in cancer: biological implications and therapeutic opportunities. Nat Rev Cancer 2010;10:9–22.
[44] Chung AS, Lee J, Ferrara N. Targeting the tumour vasculature: insights from physiological angiogenesis. Nat Rev Cancer 2010;10:505–14.
[45] Murphy EA, Majeti BK, Barnes LA, Makale M, Weis SM, Lutu-Fuga K, et al. Nanoparticle-mediated drug delivery to tumor vasculature suppresses metastasis. Proc Natl Acad Sci U S A 2008;105:9343–8.
[46] Yu Y, Wang Z-H, Zhang L, Yao H-J, Zhang Y, Li R-J, et al. Mitochondrial targeting topotecan-loaded liposomes for treating drug-resistant breast cancer and inhibiting invasive metastases of melanoma. Biomaterials 2012;33:1808–20.
[47] Oda Y, Suzuki R, Otake S, Nishiie N, Hirata K, Koshima R, et al. Prophylactic immunization with bubble liposomes and ultrasound-treated dendritic cells provided a four-fold decrease in the frequency of melanoma lung metastasis. J Control Release 2012;160:362–6.